A Multifunctional and Wireless Droop Control for Distributed Energy Storage Units in Islanded AC Microgrid Applications

Xiaofeng Sun, *Member, IEEE*, Yancong Hao, Qingfeng Wu,
Xiaoqiang Guo, *Senior Member, IEEE*, and Baocheng Wang

***Abstract*—A multifunctional and wireless droop control method for distributed energy storage units (DESUs) in ac microgrids is presented in this paper. This paper achieves the state-of-charge (SoC) balancing by employing the SoC-based *P-f* droop control method locally for the purpose to prolong the service life of DESUs and effectively utilizing the available capability of the DESUs. Besides, inspired by the conventional *P-f* droop control, a $\int Qdt - V$ droop control is proposed in this paper to eliminate the reactive power sharing errors. The $\int Qdt - V$ droop control is realized by reducing the voltage proportional to the integration of the reactive power instead of the reactive power itself. Meanwhile, the voltage compensation term which is proportional to the integration of the accurately shared active power is added to this method in order to restore the voltage to the acceptable range. The control strategy is straightforward to implement and does not require communication links as well as the gain scheduling. This paper also presents the analysis of the corresponding small-signal stability of the proposed droop control method. Simulation and experimental results are provided to validate the feasibility and effectiveness of the proposed approach.**

***Index Terms*—Distributed energy storage units, power sharing, state-of-charge balancing, voltage restoration.**

I. Introduction

MICROGRIDS based on the renewable energy resources (RES) have experienced a fast development in recent years. Microgrids are commonly comprised of RES, distributed energy storage units (DESUs), power–electronic interfaces, and electrically connected loads [1]–[6], seen in Fig. 1. The static transfer switch (STS) determines the operation modes of microgrids, i.e., grid-connected mode or autonomous islanded mode, and benefits both the utility and the customers regarding efficiency, reliability, and power quality [7]–[9].

Manuscript received August 20, 2015; revised November 2, 2015 and January 9, 2016; accepted February 1, 2016. Date of publication February 18, 2016; date of current version September 16, 2016. This work was supported by the National Natural Science Foundation of China under Award 51407155, by the National Natural Science Foundation of China under Award 51077112, by the Hebei Province Natural Science Foundation of China under Award E2015203407, and by the Hebei Province Natural Science Foundation of China under Award 13211907D-2. Recommended for publication by Associate Editor B. Lehman. *(Corresponding author: Xiaoqiang Guo.)*

The authors are with the Key Laboratory of Power Electronics for Energy Conservation and Motor Drive, Department of Electrical Engineering,Yanshan University, Qinhuangdao 066004, China (e-mail: sxf@ysu.edu.cn; haoyancong@163.com; 827211907@qq.com; gxq@ysu.edu.cn; bcwang@ysu.edu.cn).

Color versions of one or more of the figures in this paper are available online at http://ieeexplore.ieee.org.

Digital Object Identifier 10.1109/TPEL.2016.2531379

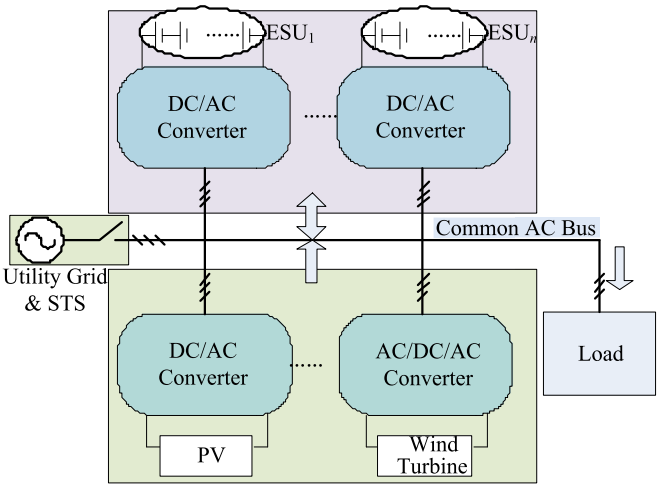

Fig. 1. Configuration of ac microgrids.

DESUs such as batteries, supercapacitor, and flywheels are very important for renewable-energy-based microgrids since they can cope with the power fluctuations caused by the intermittent and stochastic character of RES. Furthermore, the application of DESUs is also indispensible to improve the power quality and satisfy various demand side management function such as valley filling, peak shaving, black start, voltage support, etc., [10]–[18]. In the grid-connected operation, the inverters of RES and DESUs are controlled in the current control mode to supply the nondispatchable active and reactive power. Simultaneously, the microgrid voltage is dictated by the utility grid due to its large capacity. For the absence of the utility grid in the islanded operation, the DESUs which are controlled in the voltage control mode are required to regulate the voltage of the microgrid and are responsible for balancing the load with RES within their active power and reactive power limits to maintain reliability and stability of the islanded microgrids [10], [11], [14], [17], [18].

The DESUs are generally composed by the series–parallel-connected battery cells, which are also called battery string. The DESUs are connected to the common bus through power–electronically interfaced converters. Battery management system (BMS) and power converter system (PCS) are the two control systems of the DESUs [6], [19], [20]. The BMS is required to supervise the condition and to realize the state-of-charge (SoC) balancing of the battery string in a DESU. The BMS control

strategies to balance SoC among battery cells in a DESU are revealed in [20]–[23], whereas we would not focus on the BMS control as it is beyond the scope of this paper. Meanwhile, the PCS is responsible for load power sharing and SoC balancing among different DESUs. In addition to the SoC balancing in [6], [19], [24], and [25], the droop-control-based PCS control methods for DESUs are also concentrated on the coordinated control for RES and DESUs [26], [27], high-efficiency operation of DESUs [28], etc. The main objectives of this paper are to achieve the SoC balancing and the reactive power sharing of DESUs in microgrids through the PCS control.

The output power of the DESUs should be shared to avoid one certain unit prematurely running out of energy [24], [25]. Various power sharing methods have been proposed and analyzed. A concentrated control to obtain power sharing is described in [29]. This method directly adds current error to each inverter unit to compensate for the voltage reference in order to eliminate the output current errors. However, this control scheme must include a centralized controller, which limits the system expansion and redundancy. Moreover, this method highly depends on communications, which may risk a single point of fault. Droop control method is a typical decentralized control method and is often applied for power sharing without using any critical communication between inverters. In the conventional *P-f* droop control, the reactive power sharing cannot be obtained due to the mismatched line impedances and local loads, as oppose to the active power [7], [8]. In [30], an enhanced virtual impedance control scheme to achieve the reactive power sharing is proposed. The virtual line impedance can be determined according to the value of the desired line impedance and the knowledge of the physical line impedance, which needs to be estimated through either online or offline method. The accurate reactive power sharing is achieved by employing a unique approach in [31], which requires the injection of a small ac voltage signal in the system. Extracting and processing this signal may result in a complicated implementation. Also, injecting such a signal may deteriorate the output voltage and line current. Zhong [32] presents an adjustment to the reverse droop control applied in the resistive microgrid to achieve load power sharing, which, however, does not account for the effect of mismatched line impedances. An enhanced strategy is introduced in [33], which eliminates the reactive power sharing error by injecting a small real power disturbance activated by the low-bandwidth synchronization signals from the central controller and an integration term of *Q-V* droop. However, the system reliability is deteriorated due to the necessity of synchronization signal from a central controller. Communication links are developed in [34] to enhance the reactive power sharing. However, the performance of the technique is sensitive to communication delays and insignificant in the presence of local load. There is an inherent tradeoff between power sharing and voltage/frequency regulation of the droop-control-based methods [35]. In order to compromise this inherent tradeoff, a centralized secondary controller was proposed in [36] to eliminate the voltage deviation in dc microgrids. However, the voltage restoration cannot be achieved if there is a failure in the centralized controller. For higher reliability, a distributed secondary network control system is used in [4] to ensure the reactive power sharing and restore the frequency/voltage of the microgrids.

However, the accurate power sharing for DESUs could not yet fulfill SoC balancing accounting for the different initial SoC. A central control method for SoC balancing is implemented in [37]. However, this method is implemented by employing the central controller, which is not suitable for the dispersedly composed microgrids. As the DESUs are dispersedly connected to the common bus, droop control and its variants would be preferable in the microgrid applications [38]–[40]. The droop-control-based cooperative strategies can be classified into two manners: distributed manner and fully decentralized manner [28]. The control strategies in distributed manner require the parameters obtained through a local communication network or neighbor-to-neighbor communication link. In [24], a multiagent system with a frequency scheduling droop control is proposed to achieve SoC balancing for DESUs in ac microgrids. The frequency scheduling modifies the frequency by adding the items with respect to the values and average value of SoCs for all DESUs. The average value of SoCs is available through neighbor-to-neighbor communication, which is a distributed fashion and less expensive. Correspondingly, a distributed multiagent-based algorithm is proposed to achieve SoC balancing in dc microgrids by voltage scheduling, in which the voltage command is adjusted by the parameter information obtained through neighbor-to-neighbor communication. The transferred parameter is the ratio of one certain DESU to the average SoC of all the other units [25]. On the other hand, the strategies in fully decentralized manner use the local available information without communication, which are more robust and cost effective. Lu *et al.* [6] propose a method in dc microgrid to achieve SoC balancing and equalize their output power only during the discharging period, in which the droop gain is inversely proportional to the *n*th order of SoC. Lu *et al.* [19] supplement the SoC balancing method during the charging period, as the further study of [6]. The droop gain during the charging period in [19] is proportional to the *n*th order of SoC, as the supplementary of [6]. However, the design difficulty is increased in this gain scheduling methods since droop control coefficients have strong influence on the system stability [41]. The droop-control-based SoC balancing methods in decentralized manner have been studied in dc microgrids and its applications in ac microgrids need further study.

In this paper, a fully decentralized method for the SoC balancing and the reactive power sharing in ac microgrid applications is proposed, which is without communication links as well as gain scheduling compared to the previously proposed method so far. The SoC balancing and the reactive power sharing are realized by introducing the SoC-based *P-f* droop control and the $\int Qdt - V$ droop control, respectively. A voltage restoration algorithm is introduced into this control method to compromise the inherent tradeoff between the voltage regulation and the load sharing accuracy of the droop method. This voltage restoration algorithm adopts the integration of active power as the locally compensation term to restore the voltage magnitude to the acceptable range, i.e., $\pm 5\%$ [42].

The rest of this paper is organized as follows. Section II illustrates the estimation algorithm of SoC for DESUs, analyzes

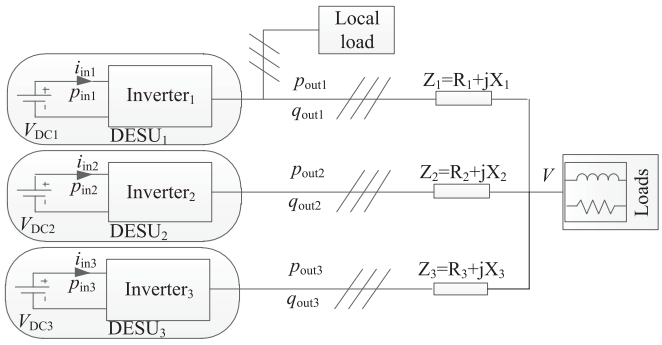

Fig. 2. Structure of parallel-connected DESUs.

the transient response of conventional *P-f* droop control, and introduces the SoC-based *P-f* droop method to achieve SoC balancing. Section III presents the $\int Qdt - V$ droop control to maintain the reactive power sharing. Section IV shows a voltage compensation method to ensure that the voltage of PCC is within the acceptable range. The small-signal stability analysis is revealed in Section V followed by the simulation and experimental verification of the proposed droop control in Section VI and Section VII, respectively. Then, Section VIII reviews the conclusion of this paper.

II. SoC-Based *P-f* Droop Control Technique

Multiple DESUs are usually dispersed and parallel operated to enhance the reliability and increase the power capacity of the energy storage system [24]. The structure of paralleled DESUs is shown in Fig. 2, where $V_{\mathrm{DC}i}$ ($i = 1, 2, 3$) is the output voltage of the *i*th DESU; $i_{\mathrm{in}i}$ is the input current of the *i*th interfacing converter (output current of the *i*th DESU); $p_{\mathrm{in}i}$ is the input power of the *i*th interfacing converter (output power of the *i*th DESU); $p_{\mathrm{out}i}(q_{\mathrm{out}i})$ is the output active (reactive) power of the *i*th interfacing converter; Z_i is the line impedance of the *i*th interfacing converter; and R_i (X_i) is the resistance (reactance) of Z_i.

A. Estimation of the SoC for DESUs in Autonomous Microgrids

To get the corresponding knowledge of DESUs, the estimation algorithm of the SoC is achieved first through the basic coulomb counting method as shown

$$\mathrm{SoC} = \mathrm{SoC}_0 - \frac{\int i_{\mathrm{in}} dt}{Ce} \tag{1}$$

where SoC_0 is the initial value of SoC and Ce denotes the capacity of a certain DESU.

The output voltage of each DESU can be regarded as constant, for the slow change of SoC and the stability of output voltage of each DESU in a large range of SoC [5], [6]. Furthermore, assuming that the DESUs are in the same voltage level, it yields

$$V_{\mathrm{DC}1} = V_{\mathrm{DC}2} = V_{\mathrm{DC}3} = V_{\mathrm{DC}}. \tag{2}$$

Meanwhile, in view of the conservation of energy in the input and output side of the power–electronically interfaced converters, it yields

$$p_{\mathrm{out}} \approx p_{\mathrm{in}} = V_{\mathrm{DC}} i_{\mathrm{in}i}. \tag{3}$$

Combing (1) with (2) and (3), it is derived

$$\mathrm{SoC} = \mathrm{SoC}_0 - \frac{\int i_{\mathrm{in}} dt}{Ce} = \mathrm{SoC}_0 - \frac{\int p_{\mathrm{out}} dt}{V_{\mathrm{DC}} Ce}. \tag{4}$$

As shown in (4), the SoC is strongly influenced by SoC_0 and the output active power of inverters. In other words, appropriate controlling against the output active power of inverters is beneficial to achieve the SoC balancing among the DESUs.

B. Review of Conventional Droop Control

By mimicking the parallel operation characteristic of synchronous generators, the frequency and voltage droop control is employed for active and reactive power regulation [7], which is expressed as

$$\omega = \omega_0 - D_P P \tag{5}$$

$$E = E_0 - D_Q Q \tag{6}$$

where ω and E are the angular frequency and the magnitude of the output voltage reference, respectively; ω_0 and E_0 are the angular frequency and the magnitude of the output voltage at no load, respectively; P and Q are the average value of active power p_{out} and reactive power q_{out} of inverters, respectively; and D_P and D_Q are the slope of droop characteristics.

Omitting the resistance of the line impedance and assuming that the power angle δ is small enough, the active and reactive power flow in Fig. 2 are shown in (7) and (8), respectively. The droop method in microgrids is based on the power flow between two nodes across the line impedance

$$P = \frac{V_{\mathrm{PCC}} \cdot E \cdot \delta}{X} \tag{7}$$

$$Q = \frac{V_{\mathrm{PCC}}(E - V_{\mathrm{PCC}})}{X} \tag{8}$$

where V_{PCC} and E are the magnitudes of PCC voltage and inverter output voltage, and X is the reactance of line impedance. For the simplicity of the detail description, it is worthy to be noted that t_- and t_+ are the moment before and after time t, respectively. The power angle at t_+ is illustrated as

$$\delta_{t_+} = \int_0^{t_-} \omega dt. \tag{9}$$

With the droop method determined in (5), the frequency decreases with the increase of active power. The power angle δ in (9) reduces subsequently, which causes the declining of the active power in turn according to (7). Assuming that the output active powers of the three parallel-connected inverters are defined as P_1, P_2, and P_3, the relationship between them is $P_3 < P_2 < P_1$. According to (5), the frequencies (ω_3, ω_2, ω_1) satisfy $\omega_3 > \omega_2 > \omega_1$, which results in more decrease of δ_1 than the others. Subsequently, P_1 reduces gradually, while P_3 increases to supply the common load. Gradually, the active powers are equally shared in the steady state. Since the frequency of the

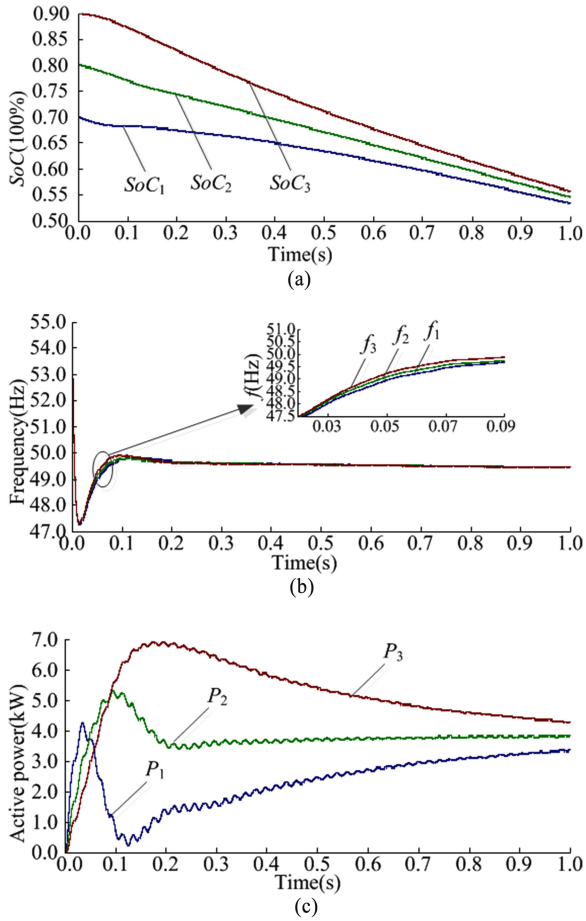

Fig. 3. Theoretical transient response of the SoC balancing method. (a) SoCs of the DESUs. (b) Output voltage frequencies of the three inverters. (c) Output active powers of the three inverters.

microgrid is unified throughout the whole system once steady-state conditions are reached, the output real powers are shared accurately between the inverters even with the mismatched line impedances.

C. SoC-Based P-f Droop Control

Inspired by the transient response of conventional frequency droop method, we propose the SoC-based *P-f* droop method to achieve SoC balancing as

$$\omega = \omega_0 - K_P P - K_{\mathrm{SoC}}(1 - \mathrm{SoC}) \tag{10}$$

where K_P and K_{SoC} are the droop coefficient of the SoC-based droop control method.

Similar to the transient response of the frequency droop method, the third term of (10) determines that the frequency of the DESU with higher SoC droops less as compared with the ones with lower SoC. As a result, the DESU with higher SoC delivers larger active power compared with the ones with lower SoC, which is beneficial to SoC balancing of DESUs. The second term of (10) guarantees the active power sharing as analyzed before. Equation (4) implies that the active power is the slope of SoC, so accurately shared active power is necessary for SoC balancing. Given that the three paralleled DESUs with different initial SoCs and line impedances are parallel connected, Fig. 3 describes the transient response of them controlled by the SoC-based *P-f* droop method. It can be seen from Fig. 3(a) and (b) that the DESU with larger SoC presents higher frequency (larger power angle according to (9)) in the transient response than the others. Then, the DESU with higher SoC delivers more active power according to (7), shown in Fig. 3. Considering the estimation of SoC in (4), the SoCs become balanced gradually under the control of the SoC-based *P-f* method.

III. Proposed Reactive Power Sharing Control Algorithm

Load power sharing is one of the significant aspects in the development of autonomous microgrids. However, since the reactive power of each inverter depends on the voltage amplitudes due to the *Q–V* droop, the reactive power sharing between the inverters becomes undesirable.

Combing (5) with (7) and (9), the output active power at t_+ is

$$P_{t_+} = \frac{V_{\mathrm{PCC}} E \int_0^{t_-} (\omega_0 - D_P P)dt}{X} \tag{11}$$

where P_{t+} is the active power at t_+. Equation (11) depicts that the output active power of the inverter with conventional droop method is regulated by the historical information of active power. Similarly, combining (6) with (8), we obtained

$$Q = \frac{V_{\mathrm{PCC}}(E_0 - V_{\mathrm{PCC}})}{X + V_{\mathrm{PCC}} D_Q}. \tag{12}$$

Equation (6) presents that the conventional *Q–V* droop method reduces the voltage proportionally to the current value of the reactive power instead of the historical information of it which results in (12). It can be seen from (12) that the output reactive power in (12) is totally determined by the immediate voltage and line impedances instead of the historical information of the reactive power. Different from (5), the voltage in (6) cannot carry the information of the reactive power conditions. Once the steady state is reached, different inverters will operate at different positions on the voltage droop curve, resulting in the unshared reactive powers. The relationship of conventional *Q–V* droop in (6) and the reactive power transmission in (8) is shown in Fig. 4, taking two DESUs (DESU_1/DESU_2) with mismatched line impedances for example. The solid line represents the droop control curve. The black and red dashed lines stand for the power flow curves with the 311-V and 305-V PCC voltages, respectively. In addition, the slope of the power flow curve with larger line impedance is larger in Fig. 4. It shows that the reactive power errors (Q_{error1}, Q_{error2}) cannot be eliminated under the conventional droop control.

Imitating the power flow of conventional *P-f* droop control, the historical information of reactive power is injected into the *Q–V* droop method artificially, being called the $\int Qdt - V$ droop control, as can be seen in

$$E_{t_+} = E_0 - K_Q \int_0^{t_-} Q dt \tag{13}$$

where E_{t+} is the magnitude of the output voltage reference at t_+ and K_Q is the coefficient of the $\int Qdt - V$ droop control.

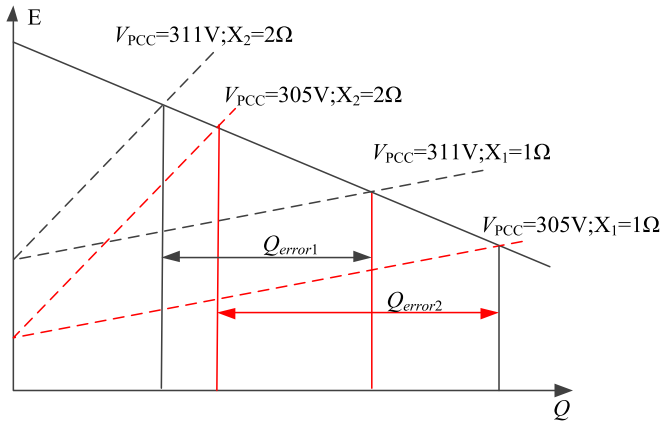

Fig. 4. Relationship of Q–V droop and reactive power transmission.

Substituting (13) into (8), it yields

$$Q_{t_+} = \frac{V_{\mathrm{PCC}}(E_0 - K_Q \int_0^{t_-} Q dt - V_{\mathrm{PCC}})}{X} \tag{14}$$

where Q_{t+} is the output reactive power at t_+

Equation (14) demonstrates that the reactive power flow of the $\int Qdt - V$ droop method is strongly influenced by the historical information of the reactive power. The reference voltage magnitude in (13) carries the information of the reactive power and determines the output voltage magnitude to achieve the reactive power sharing. More specifically, with the $\int Qdt - V$ droop method, the voltages of DESUs delivering more reactive powers will decrease more than the others. The theoretical transient responses of the $\int Qdt - V$ droop method are presented in Fig. 5. Fig. 5(a) illustrates the relationship between the $\int Qdt - V$ droop and the reactive power transmission. The intersections of the black lines imply the operation point at t_1. Meanwhile, the intersections of the red lines present the operation point at t_2 ($t_1 < t_2$). ΔE_1 and ΔE_2 stand for the voltage droops of DESU_1 and DESU_2 from t_1 to t_2, respectively. It is obvious that $\Delta E_1 > \Delta E_2$, which results in the decrease of reactive power error ($Q_{\mathrm{errort}2} < Q_{\mathrm{errort}1}$). Fig. 5(b) and (c) describes the voltage and the reactive power error, respectively. It can be seen from Fig. 5(b) that different extents of voltage droops are demonstrated to decrease the reactive power error. Fig. 5(c) shows that the output reactive powers of DESUs are gradually shared.

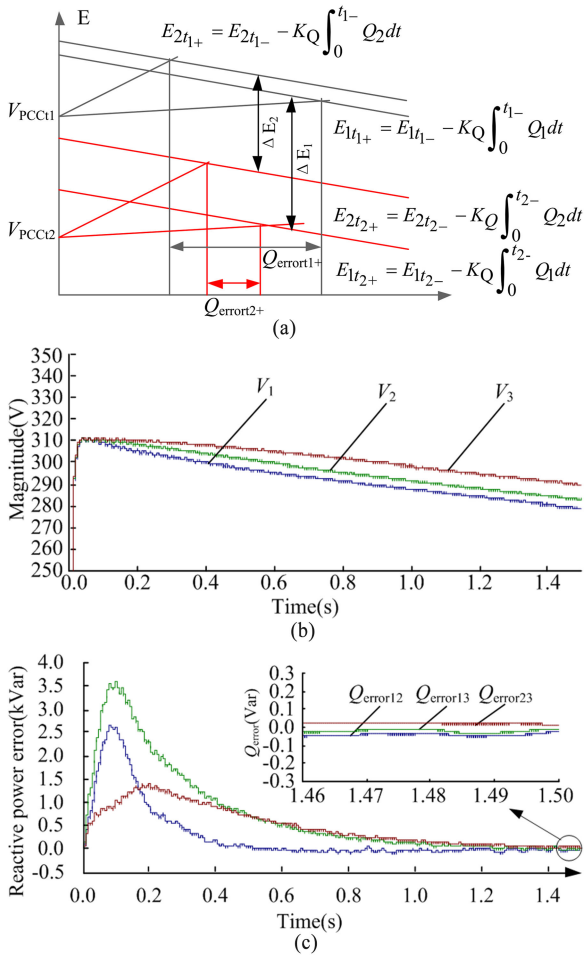

Fig. 5. Theoretical transient response of reactive power sharing. (a) Relationship of $\int Qdt - V$ droop and reactive power transmission. (b) Output voltage magnitudes of the three inverters. (c) Reactive power errors.

IV. Voltage Restoration

In the grid-connected mode, the voltage of the microgrid is dominated by the main grid due to the large capacity of the utility grid. Hence, the main task of the microgrid in this mode is to deliver the scheduled power. In the islanded mode, it is necessary to not only dispatch the real and reactive power among the inverters but also maintain the voltage magnitude to a certain allowable range, i.e., ±5% [42]. In autonomous microgrids, one of the main tasks of the DESUs is to keep the voltage magnitudes in the allowable range [17], [18], [42], whereas there is an inherent tradeoff between the voltage accuracy and power sharing existing in the proposed droop method. Hence, voltage restoration without communication links should also be employed into the control of the DESUs, simultaneously. Taking full advantage of the accurately shared active power, a compensation term proportional to the integration of the active power is added to (13), which can be expressed as

$$E_{t_+} = E_0 - K_Q \int_0^{t_-} Q dt + K_{\mathrm{PV}} \int_0^{t_-} P dt \tag{15}$$

where K_{PV} is the voltage compensation coefficient.

The employment of the active power integration will not influence the performance of the reactive power sharing. As explained in Section III, the reactive power sharing is achieved through reducing the voltage by different extents. As aforementioned, the active powers are evenly shared due to the unified frequency and nearly decoupled with the reactive powers in the case of the high *X*/*R* ratio line impedances. According to (15), the same voltage compensation term is added to the voltage reference without affecting the different extents of voltage droops to achieve reactive power sharing. More specifically, the second term in (15) employs different extents of output voltage droops to obtain the reactive power sharing. Meanwhile, the third term in (15) compensates the voltage by the same extent to restore the

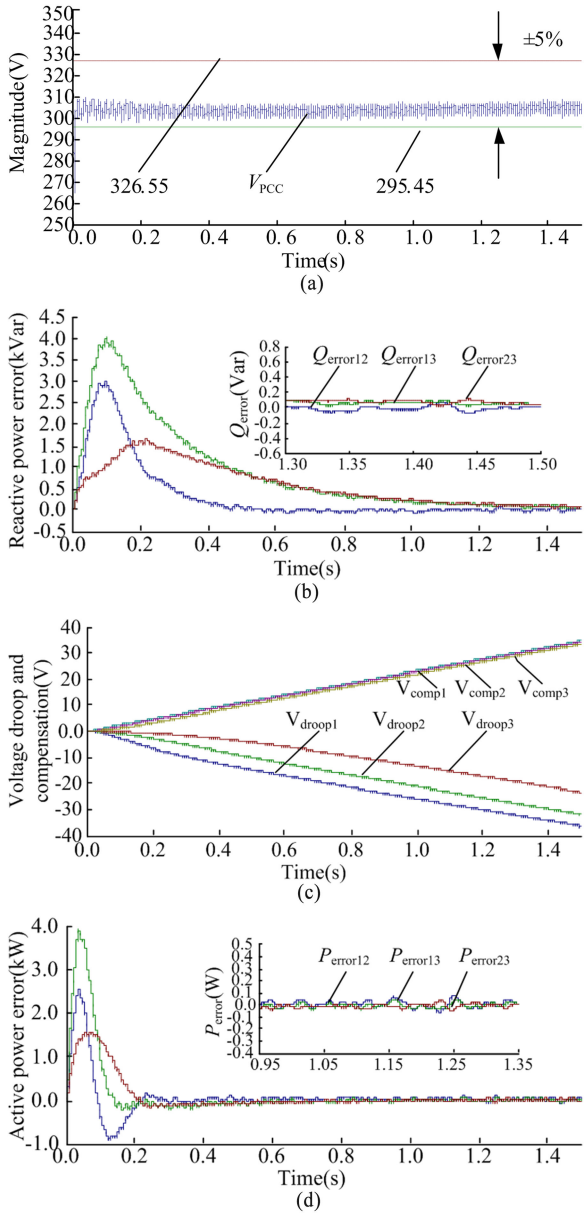

Fig. 6. Regulation process of voltage restoration and reactive power sharing. (a) Magnitude of PCC voltage. (b) Reactive power errors. (c) Different voltage droops and the same compensation. (d) Active power errors.

voltage to the acceptable range. Thus, both the reactive power sharing and voltage restoration are satisfied by (15). The voltage restoration together with reactive power sharing regulation process of a system with three paralleled DESUs is described in Fig. 6. Fig. 6(a) shows that the magnitude of PCC voltage is restored to the acceptable range. It can be seen in Fig. 6(c) that different extents of voltage droops are implemented to achieve the reactive power sharing and the same voltage compensation is added to restore the voltage magnitude. From Fig. 6(b) and (d), we can see that the reactive powers are equally shared without disturbing the active power sharing.

Combing (10) with (15), the whole control structure of the inverters is presented in Fig. 7, in which different models confined by specific dashed lines represents their respective functions in

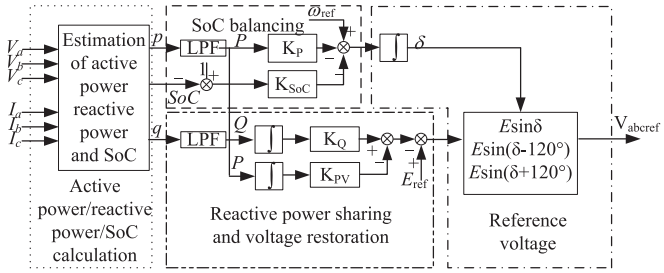

Fig. 7. Control structure of the inverters.

the control structure. The output variable $V_{abc\mathrm{ref}}$ stands for the reference voltage in three phases, which are then sent to the inner voltage loop for the output voltage to track.

V. Small-Signal Stability Analysis

In this section, a small-signal analysis is proposed to investigate the influence of the multifunctional and wireless droop control coefficients on the stability and transient response, which provides a guideline for the designers to choose a proper value. For the sake of the safe and efficient operation of the converters, the droop control coefficients are first confined within the limits as follows:

$$|\Delta\omega_{\max}|/P_{\max} < K_P < |\Delta\omega_{\max}|/P_{\min}$$
$$|\Delta\omega_{\max}|/(1-\mathrm{SoC}_{\max}) < K_{\mathrm{SoC}} < |\Delta\omega_{\max}|/(1-\mathrm{SoC}_{\min})$$
$$|\Delta E_{\max}|/Q_{\max} < K_Q < |\Delta E_{\max}|/Q_{\min}$$
$$|\Delta E_{\max}|/P_{\max} < K_{\mathrm{PV}} < |\Delta E_{\max}|/P_{\min}.$$

Particularly, K_Q and K_{PV} in (15) are further confined by the voltage restoration. K_Q and K_{PV} determine the extents of the voltage droops and compensation, respectively. Theoretically speaking, K_{PV} does not influence the reactive power sharing performance since the reactive power sharing is achieved by employing the different extents of voltage droops introduced by the unshared reactive power. Due to the evenly shared active power, K_{PV} only introduce the same extent of voltage compensation, which does not affect the different extents of voltage droops. Hence, the reactive power sharing has little impact on choosing the coefficient. However, the voltage restoration is sensitive to K_Q and K_{PV}. Assuming that the evenly shared reactive and active powers in the steady state are Q_{share} and P_{share}, the voltage restoration in (15) requires that

$$K_Q\int_0^{t_-} Q_{\mathrm{share}}dt = K_Q\int_0^{t_-}(Q_L/n)dt$$
$$\approx K_{\mathrm{PV}}\int_0^{t_-}(P_L/n)dt = K_{\mathrm{PV}}\int_0^{t_-}(P_{\mathrm{share}})dt \quad (16)$$

where Q_L and P_L are the reactive and active power of the load, respectively, and *n* implies the number of converters.

It is can be derived from (16) that

$$K_Q/K_{\mathrm{PV}} \approx \int_0^{t_-} P_L dt \Big/ \int_0^{t_-} Q_L dt \approx P_L/Q_L. \quad (17)$$

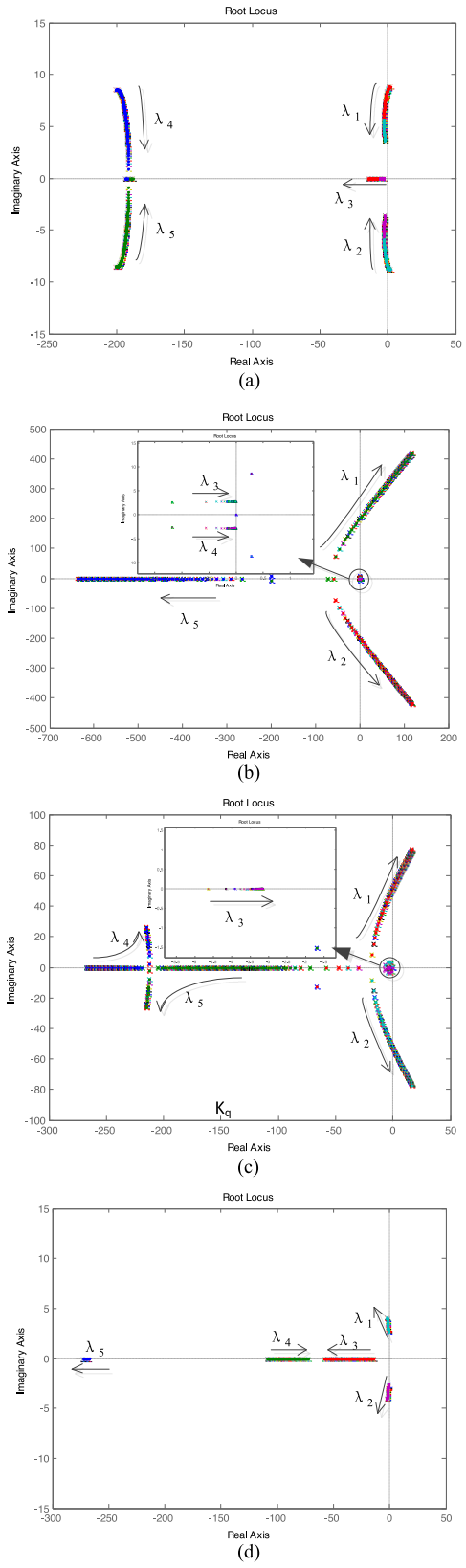

Fig. 8. Root locus diagrams for droop control coefficient values. (a) Root locus for $0 \le K_P \le 1.88e-3$, $K_Q = 1e-5$, $K_{\mathrm{SoC}} = 6.28e-6$, $K_{\mathrm{PV}} = 6e-6$. (b) Root locus for $0 \le K_Q \le 1e-4$, $K_P = 1.88e-6$, $K_{\mathrm{SoC}} = 6.28e-6$, $K_{\mathrm{PV}} = 6e-6$. (c) Root locus for $0 \le K_{\mathrm{SoC}} \le 6.28e-5$, $K_P = 1.88e-6$, $K_Q = 1e-5$, $K_{\mathrm{PV}} = 6e-6$. (d) Root locus f or $0 \le K_{\mathrm{PV}} \le 6e-5$, $K_P = 1.88e-6$, $K_Q = 1e-5$, $K_{\mathrm{SoC}} = 6.28e-6$.

TABLE I
PARAMETERS OF THE PROPOSED DROOP CONTROL METHOD

Item	Symbol	Nominal value	Units
Filter cutoff frequency	ω_c	200	rad/s
Nominal amplitude of output voltage	E	311	V
Nominal amplitude of PCC voltage	V_{PCC}	311	V
Initial phase difference	δ	0.17	rad
Line impedance	X	1	Ω
DC-link voltage	V_{DC}	800	V
Capacity of DESU	Ce	100	Ah
Item	**Symbol**	**Variation Range**	**Units**
Droop Coefficient	K_P	0 to 1.88e–3	rad/W
Droop Coefficient	K_Q	0 to 1e–4	V/var
Droop Coefficient	K_{SoC}	0 to 6.28e–5	rad
Compensation Coefficient	K_{PV}	0 to 6e–5	V/W

It is can be seen from (17) that in addition to the confined limits above, the relationship of K_{PV} and K_Q is related to the load powers.

By setting up the small-signal model of the proposed droop method, the root locus corresponding to the aforementioned coefficient range can be derived. According to the root locus, the desired value of the coefficients within their respective range can be picked out.

Modeling the low-pass filters with a first-order description and linearizing (7) and (8), it yields that

$$\Delta p = \frac{\omega_c}{s+\omega_c}\frac{V}{X}[\Delta e \sin\delta + \Delta\delta E\cos\delta] \tag{18}$$

$$\Delta q = \frac{\omega_c}{s+\omega_c}\frac{V}{X}[\Delta e \cos\delta + \Delta\delta E\sin\delta] \tag{19}$$

where Δ denotes perturbed values, capital letters represent equilibrium point values, X is the equivalent impedance including output impedance and line impedance, etc., and ω_c is the cutoff angular frequency of the low-pass filters.

Subsequently, irrespective of the time in (10) and (15), by perturbing and linearizing the proposed droop method shown in (10) and (15), we obtain

$$\Delta\omega = -K_P\Delta p + K_{\mathrm{SoC}}\Delta\mathrm{SoC} \tag{20}$$

$$\Delta e = -\frac{K_Q}{s}\Delta q + \frac{K_{\mathrm{PV}}}{s}\Delta p \tag{21}$$

since

$$\Delta\omega(s) = s\Delta\delta(s) \tag{22}$$

and

$$\Delta\mathrm{SoC} = -\frac{1}{sV_{\mathrm{DC}}Ce}\Delta p. \tag{23}$$

Substituting (22) and (23) into (20), we have

$$\Delta\delta = -\frac{1}{s}(K_P + \frac{K_{\mathrm{SoC}}}{sV_{\mathrm{DC}}Ce})\Delta p. \tag{24}$$

Considering (18) with (19), (21), and (24), it can be found that

$$s^5\Delta\delta + as^4\Delta\delta + bs^3\Delta\delta + cs^2\Delta\delta + e\Delta\delta = 0 \tag{25}$$

TABLE II
SYSTEM PARAMETERS

Terms		Symbol	Simulation Parameters		Experimental Parameters	
Line impedance		$R_1 + jX_1$	$0.15 + j0.5\ \Omega$		$0.2 + j1.0\ \Omega$	
		$R_2 + jX_2$	$0.3 + j1.0\ \Omega$			
		$R_3 + jX_3$	$0.6 + j2.0\ \Omega$		$0.4 + j2.0\ \Omega$	
Droop coefficient		K_P	1.88e–4 rad/W		0.0025 rad/W	
		K_Q	1e–5 V/Var		0.00155 V/Var	
		K_{SoC}	6.28e–6 rad			
Compensation coefficient		K_{PV}	6e–6 V/W		0.00935 V/W	
Common load	Case study 1	$P + jQ$	4 kW + j2 kvar		205.9 W + j300 Var	
	Case study 2		Before load change	After load change	Before load change	After load change
			4 kW + j2 kvar	6 kW + j3 kvar	205.9 W + j300 Var	205.9 W + j400 Var
With local load	Case study 3		Common load	Local load	Local load	
			4 kW + j2 kvar	2 kW + j1 kVar	j35.9 Var	

where

$$
\begin{aligned}
a &= 2\omega_c \\
b &= \omega_c^2 + \frac{E\cos\delta\omega_c V K_p + (K_Q\cos\delta - K_{\mathrm{PV}}\sin\delta)\omega_c V}{X} \\
c &= \frac{\omega_c^2 V(EK_P\cos\delta + K_Q\cos\delta - K_{\mathrm{PV}}\sin\delta)}{X} \\
&\quad + \frac{E\cos\delta\omega_c V K_{\mathrm{SoC}}}{XV_{\mathrm{DC}}Ce} \\
d &= \frac{\omega_c^2 V^2 EK_P K_Q}{X^2} + \frac{K_{\mathrm{SoC}}E\cos\delta\omega_c^2 V}{XV_{\mathrm{DC}}Ce} \\
e &= \frac{K_{\mathrm{SoC}}K_Q\omega_c^2 V^2 E}{X^2 V_{\mathrm{DC}}Ce}.
\end{aligned}
$$

Equation (25) shows the fifth-order small-signal model of the closed-loop system. Through analyzing the corresponding characteristic equation shown in (25), we can select proper coefficients in the proposed droop control method to achieve a desired small-signal stability performance.

Fig. 8 depicts the root locus diagrams using the parameters listed in Table I with a variation of the coefficients in the proposed droop method. Notice that the system has five eigenvalues (λ_1, λ_2, λ_3, λ_4, and λ_5). The two complex-conjugated poles (λ_1 and λ_2) are the dominant poles according to the location of the five poles, obtaining a second-order behavior. The arrows indicate the evolution of corresponding pole with the changing coefficients. It can be observed that the poles can be adjusted to fix the desired small-signal stability of the closed-loop system.

Fig. 8(a) shows that with the increase of K_P within the predefined range, the dominant poles (λ_1 and λ_2) move from the right half s-plane to the left, which denotes that the small-signal stability is enhanced by increasing K_P properly. Fig. 8(b) reveals that by increasing K_Q, the dominant eigenvalues (λ_1 and λ_2) move toward the unstable region making the system more oscillatory and finally leading to instability. Fig. 8(c) denotes the root locus with the increase of K_{SoC}. Similarly, neglecting the nondominant poles, the dominant eigenvalues movement trend is similar to Fig. 8(b), which may cause small-signal instability. The root locus corresponding to the changing K_{PV} is illustrated in Fig. 8(d), where the dominant poles (λ_1 and λ_2) go

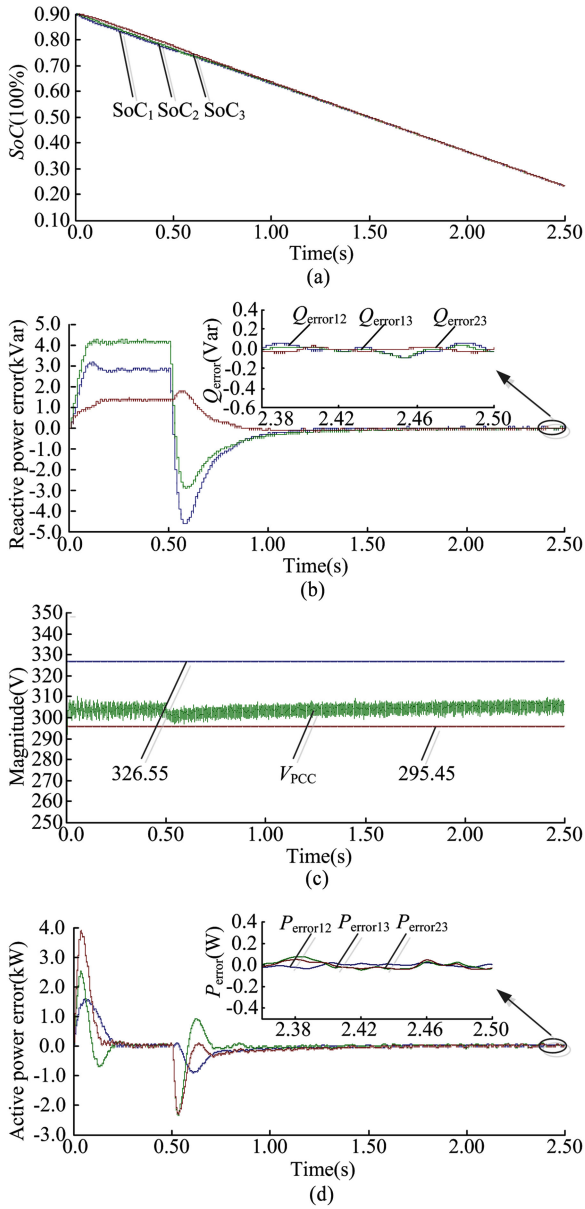

Fig. 9. Waveforms when $\mathrm{SoC}_{01} = \mathrm{SoC}_{02} = \mathrm{SoC}_{03}$. (a) SoCs of the three paralleled DESUs. (b) Reactive power errors. (c) Magnitude of the PCC voltage. (d) Active power errors.

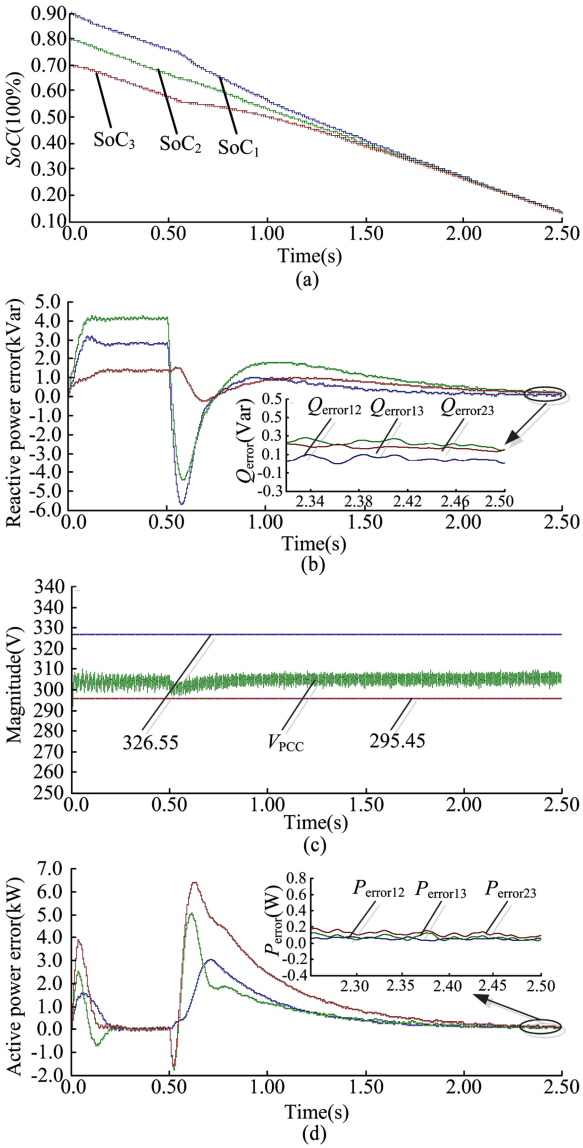

Fig. 10. Waveforms when SoC01 > SoC02 > SoC03. (a) SoCs of the three paralleled DESUs. (b) Reactive power errors. (c) Magnitude of the PCC voltage. (d) Active power errors.

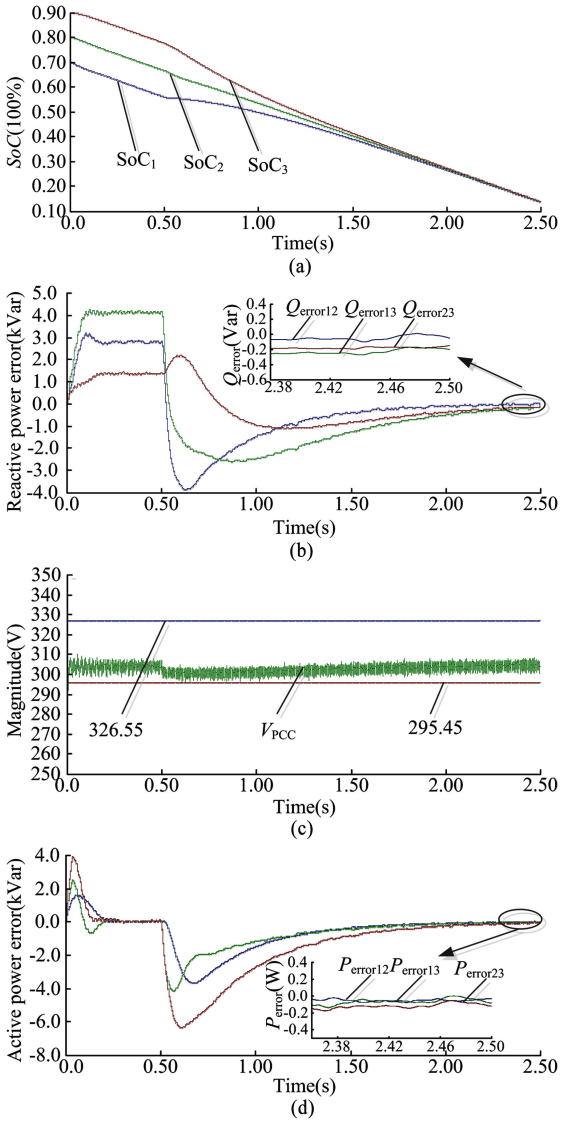

Fig. 11. Waveforms when $\mathrm{SoC}_{01} < \mathrm{SoC}_{02} < \mathrm{SoC}_{03}$. (a) SoCs of the three paralleled DESUs. (b) Reactive power errors. (c) Magnitude of the PCC voltage. (d) Active power errors.

to the left-half s-plane, resulting in better small-signal stability performance.

It has been shown in Fig. 8 that the small-signal stability of the closed-loop system for the proposed droop method is sensitive to the coefficients. We can guarantee the system stability and fine tune the dynamic performance by adjusting the droop coefficients within a wider variation of the droop coefficients. Considering the aforementioned, the coefficients K_P, K_Q, K_{SoC}, and K_{PV} in simulation are chosen as 1.88e–6, 1e–5, 6.28e–6, and 6e–6, respectively.

VI. Simulation Results

To test the feasibility and effectiveness of the proposed droop control methods, an islanded microgrid consisting of three paralleled DESUs (defined as DESU_1, DESU_2, and DESU_3) are studied. The key parameters of the system are listed in Table II. Due to the mismatched line impedances and the different initial SoCs of the system, the problems mentioned in Section I cannot be avoided. This section reveals three case studies under different conditions with the proposed droop method to further illustrate the performance of it. In each case study, there are three subcases with different conditions of initial SoC of the three parallel-connected DESUs, i.e., $\mathrm{SoC}_{01} = \mathrm{SoC}_{02} = \mathrm{SoC}_{03}$, $\mathrm{SoC}_{01} > \mathrm{SoC}_{02} > \mathrm{SoC}_{03}$, and $\mathrm{SoC}_{01} < \mathrm{SoC}_{02} < \mathrm{SoC}_{03}$, respectively. The system responses of each subcase are presented successively, which demonstrates that the proposed droop method can solve the problems induced by mismatched line impedances and different initial SoC simultaneously in the presence of load step change and local load. To test the feasibility and effectiveness of the proposed droop control methods, an islanded microgrid consisting of three paralleled DESUs (defined as DESU_1, DESU_2, and DESU_3) is studied. The key parameters of the system are listed in Table II. Due to the mismatched

TABLE III
REACTIVE POWER ERROR

Initial SoC		$SoC_{01} = SoC_{02} = SoC_{03}$			$SoC_{01} > SoC_{02} > SoC_{03}$			$SoC_{01} < SoC_{02} < SoC_{03}$		
Reactive power error (kVar)		$Q_{error12}$	$Q_{error13}$	$Q_{error23}$	$Q_{error12}$	$Q_{error13}$	$Q_{error23}$	$Q_{error12}$	$Q_{error13}$	$Q_{error23}$
Case study I	Conventional	2.804	4.066	1.302	2.798	4.098	1.300	2.824	4.069	1.295
	Improved	8.192e–6	3.173e–5	2.345e–5	4.188e–5	2.155e–4	1.734e–4	−8.770e–5	−2.371e–6	−1.782e–6

line impedances and the different initial SoCs of the system, the problems mentioned in Section I cannot be avoided. This section reveals three case studies under different conditions with the proposed droop method to further illustrate the performance of it. In each case study, there are three subcases with different conditions of initial SoC of the three parallel-connected DESUs, i.e., $SoC_{01} = SoC_{02} = SoC_{03}$, $SoC_{01} > SoC_{02} > SoC_{03}$, and $SoC_{01} < SoC_{02} < SoC_{03}$, respectively. The system responses of each subcase are presented successively, which demonstrates that the proposed droop method can solve the problems induced by mismatched line impedances and different initial SoC simultaneously in the presence of load step change and local load.

A. Case Study I: From Conventional Droop Control to Improved Droop Control

The performance of the improved droop control and the conventional droop control with unequal line impedances and different initial SoC is compared and tested in this case study. The line impedance, droop coefficients, and common load are as in Table II. Figs. 9–11 show the related outcomes (SoCs, output active error, reactive power error, and the voltage magnitude of PCC) corresponding to $SoC_{01} = SoC_{02} = SoC_{03}$, $SoC_{01} > SoC_{02} > SoC_{03}$, and $SoC_{01} < SoC_{02} < SoC_{03}$, respectively. It can be seen that during the first 0.5 s and the following 1 s, the DESUs are controlled by conventional droop control and the improved droop control, respectively. In order to evaluate the performance of the improved droop control, the reactive power errors of the three DESUs are defined as $Q_{error12} = Q_1 - Q_2, Q_{error13} = Q_1 - Q_3$, and $Q_{error23} = Q_2 - Q_3$. Similarly, the active power errors of the three DESUs are known as $P_{error12} = P_1 - P_2, P_{error13} = P_1 - P_3$, and $P_{error23} = P_2 - P_3$.

Obviously, the balanced SoC is gradually achieved shown in Figs. 9(a), 10(a), and 11(a). The reactive power errors in the steady state under the conventional droop control and the improved droop control in Figs. 9(b), 10(b), and 11(b) are listed in Table III. The improved droop control can achieve equal reactive power sharing compared to the conventional one. The voltage magnitudes are limited within the acceptable range, i.e., ±5% seen from Figs. 9(c), 10(c), and 11(c). From Figs. 9(d), 10(d), and 11(d), it can be derived that the active power sharing does not been influenced by the reactive power sharing and voltage restoration.

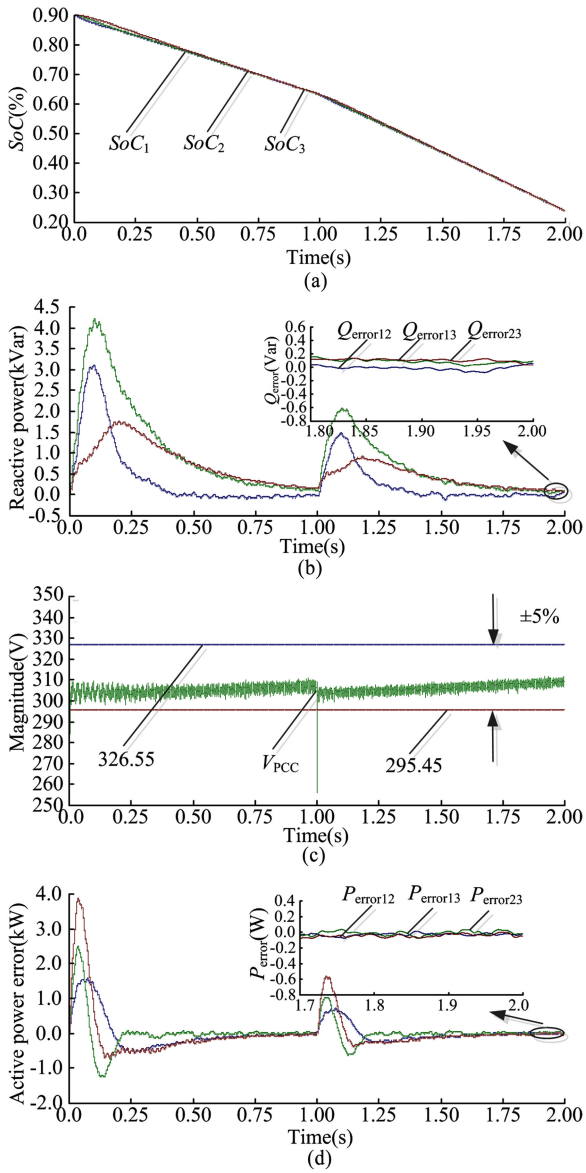

Fig. 12. Waveforms when $SoC_{01} = SoC_{02} = SoC_{03}$. (a) SoCs of the three paralleled DESUs. (b) Reactive power errors. (c) Magnitude of the PCC voltage. (d) Active power errors.

B. Case Study II: Load Step Change of Both Active and Reactive Power

In this section, we shall investigate the capability of the proposed droop method to achieve SoC balancing, power sharing, and voltage restoration confronted with a load change of both active and reactive power from 4 kW + *j*2 kvar to 6 kW + *j*3 kvar. Figs. 12–14 provide the system performance (SoCs, output active error, reactive power error, and the voltage magnitude of PCC) corresponding to $SoC_{01} = SoC_{02} = SoC_{03}$, $SoC_{01} > SoC_{02} > SoC_{03}$, and $SoC_{01} < SoC_{02} <$

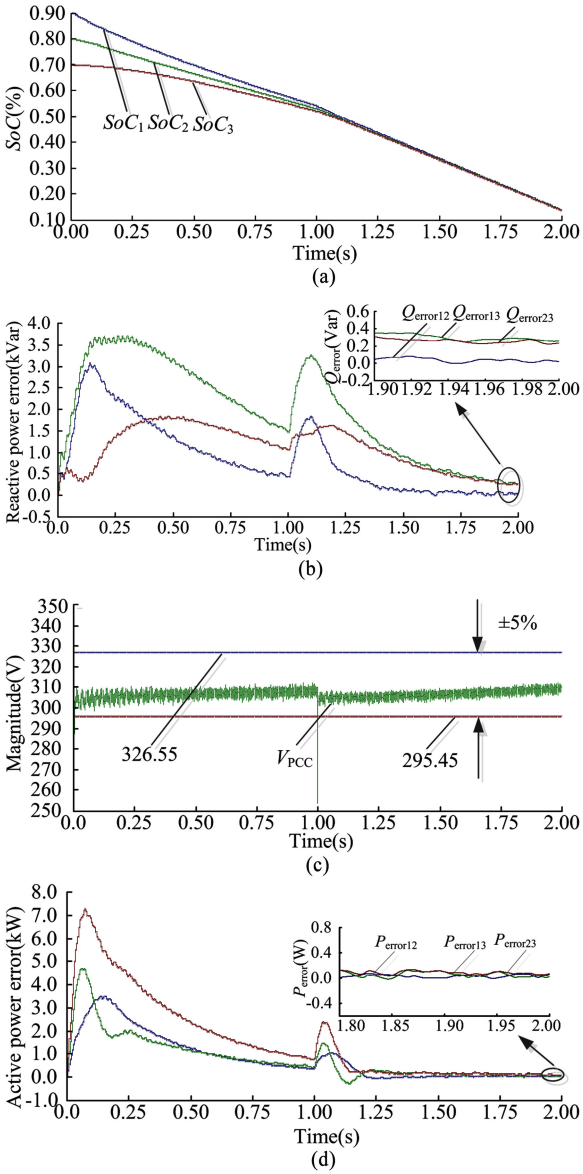

Fig. 13. Waveforms when $\mathrm{SoC}_{01} > \mathrm{SoC}_{02} > \mathrm{SoC}_{03}$. (a) SoCs of the three paralleled DESUs. (b) Reactive power errors. (c) Magnitude of the PCC voltage. (d) Active power errors.

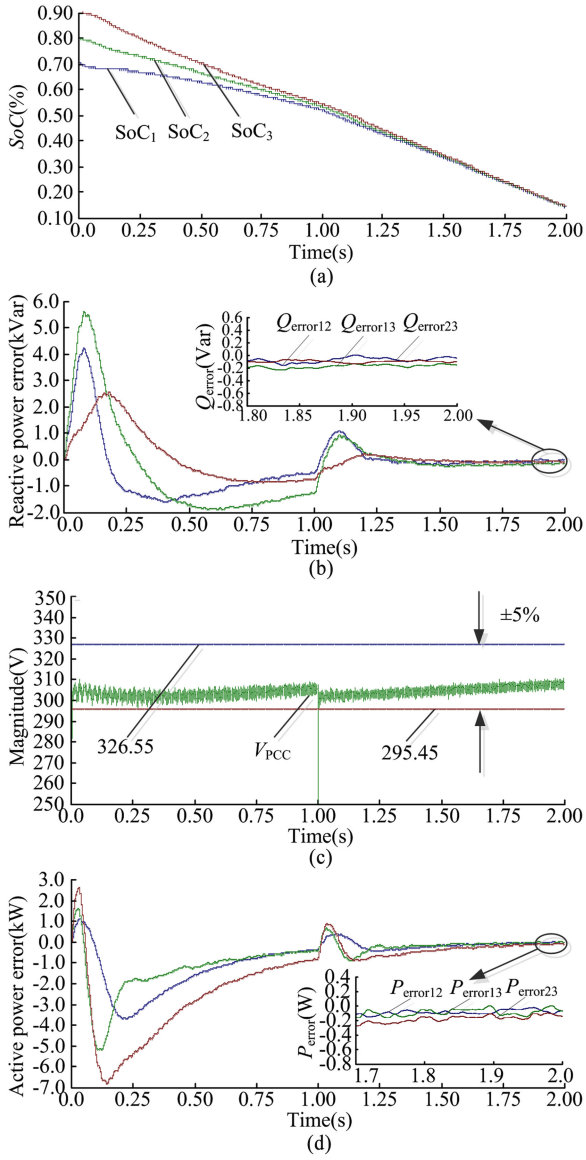

Fig. 14. Waveforms when $\mathrm{SoC}_{01} < \mathrm{SoC}_{02} < \mathrm{SoC}_{03}$. (a) SoCs of the three paralleled DESUs. (b) Reactive power errors. (c) Magnitude of the PCC voltage. (d) Active power errors.

SoC_{03} when both the active and reactive power change at 1.0 s, respectively.

It is demonstrated that with the proposed droop methods, SoC balancing, power sharing, and voltage restoration can be achieved regardless of the load step change of both the active and reactive power.

C. Case Study III: Local Load

In the autonomous microgrid, the location of the local loads will affect the power flows. Since the frequency of the microgrid is the same in the steady state, the active power sharing is not influenced by the local loads. However, the reactive power sharing performance is strongly affected by the local loads. In order to further illustrate the effectiveness of the proposed droop method, the corresponding outcomes are revealed in the presence of 2 kW $+ j1$ kVar local load in DESU_1.

The figures above demonstrate that the proposed droop method can achieve SoC balancing, reactive power sharing, and voltage restoration in the presence of local load, which further validates the effectiveness of this method.

VII. Experimental Results

In this section, the proposed control method is tested under a system with two paralleled inverters. Two dc power sources are used as the battery simulators by embedding (4) in the DSP program to calculate the SoCs of the virtual DESUs. The simplified diagram of the three-phase experimental setup is shown in Fig. 2 without the DESU_3. The experimental parameters are listed in Table II. The paralleled inverters are digitally

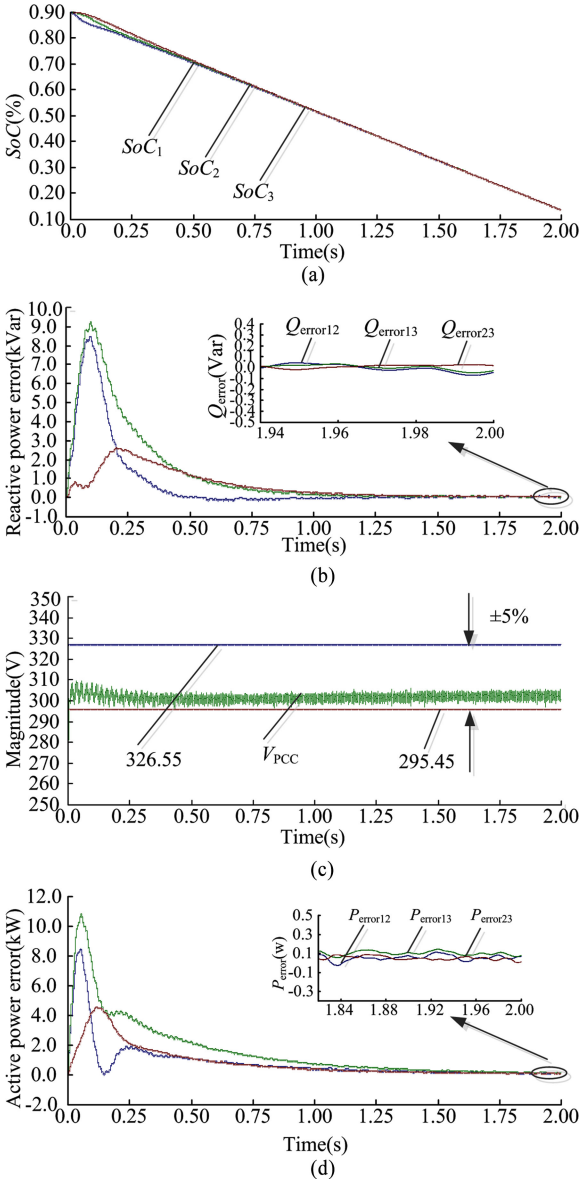

Fig. 15. Waveforms when $\mathrm{SoC}_{01} = \mathrm{SoC}_{02} = \mathrm{SoC}_{03}$. (a) SoCs of the three paralleled DESUs. (b) Reactive power errors. (c) Magnitude of the PCC voltage. (d) Active power errors.

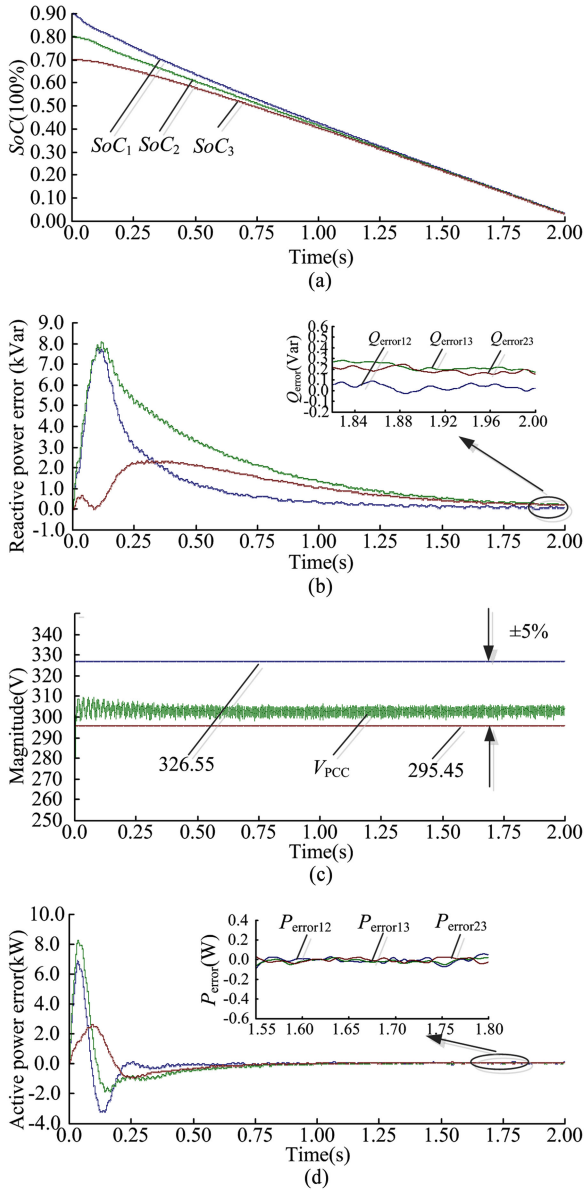

Fig. 16. Waveforms when $\mathrm{SoC}_{01} > \mathrm{SoC}_{02} > \mathrm{SoC}_{03}$. (a) SoCs of the three paralleled DESUs. (b) Reactive power errors. (c) Magnitude of the PCC voltage. (d) Active power errors.

controlled by TMS320F2812 fixed-point DSP to implement the power and voltage control algorithm. The line impedances of the two DESUs are set as $0.2 + j1\ \Omega$ and $0.4 + j2\ \Omega$, respectively. Meanwhile, the local load is located in DESU_1. The reactive power sharing, the voltage restoration, and the SoC balancing with different initial SoC are validated successively and experimentally in this section.

A. Reactive Power Sharing

Case study I: In this case, the two paralleled inverters are controlled by the conventional droop method before 20 s. At $t = 20$ s, the control method is switched from the conventional droop control to the $\int Qdt - V$ droop control. The stages of the control methods are labeled on the top of the figures, so as the following figures. The reactive and active powers of the two inverters are shown in Fig. 18(a), which reveals that the reactive powers are not equally shared under the conventional droop control due to the mismatched line impedances and subsequently shared under the $\int Qdt - V$ droop control. It is also can be seen from Fig. 18(a) that the active powers are properly shared due the same system frequency. Fig. 18(b) gives the voltages of the two inverters. Under the conventional droop control, the voltages do not deviate from the nominal value due to the small droop coefficients. In the $\int Qdt - V$ droop control, the reactive power sharing is achieved at the price of deviation of voltage magnitude, which requires the voltage restoration scheme.

Case study II (*load step change*): In order to further validate the effectiveness of the proposed $\int Qdt - V$ droop method,

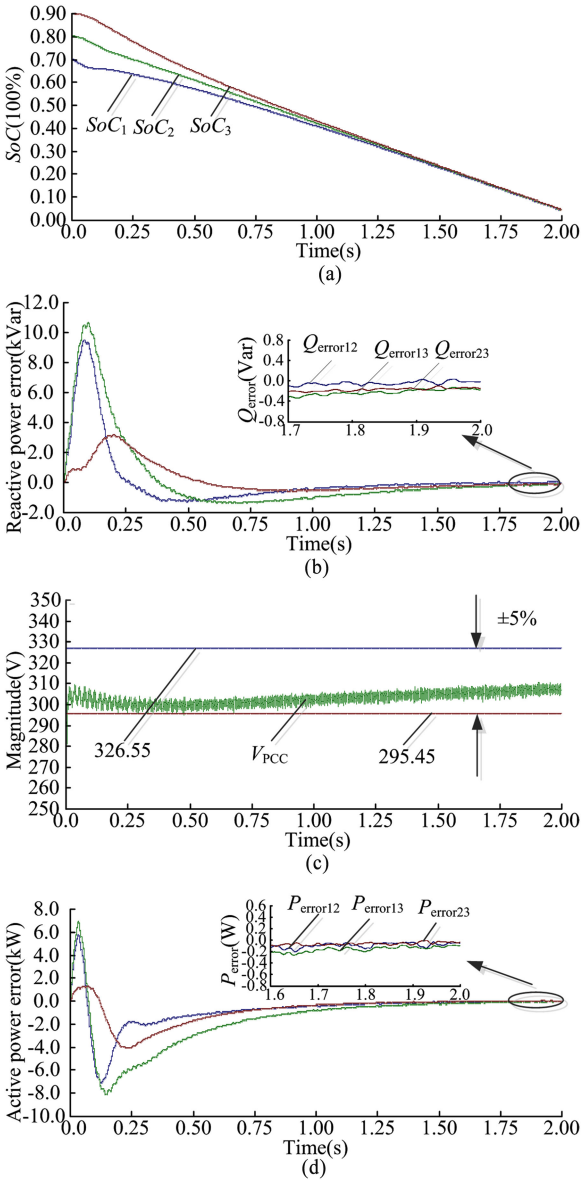

Fig. 17. Waveforms when $\mathrm{SoC}_{01} < \mathrm{SoC}_{02} < \mathrm{SoC}_{03}$. (a) SoCs of the three paralleled DESUs. (b) Reactive power errors. (c) Magnitude of the PCC voltage. (d) Active power errors.

the response of the proposed droop method when the common load changes suddenly at $t = 25.6$ s and returns back to the original common load at $t = 33.6$ s is shown in Fig. 19. The stages of the control methods are labeled on the top of figures. Fig. 19(a) shows that under the $\int Qdt - V$ control method, the reactive powers are equally shared even with the double-changed common load. Similar to Fig. 18(b), the voltages in Fig. 19(b) sacrifice to achieve the reactive power sharing.

Case study III (*local load*): Since the performance of the reactive power sharing is strongly influenced by the local load, the $\int Qdt - V$ droop method is demonstrated with local load in this section. The corresponding local load is located in DESU_1. Fig. 20 shows the reactive powers and output voltages of the two inverters. The stages of the control methods are labeled on the top of Fig. 20. Compared with Fig. 18(a), the reactive power

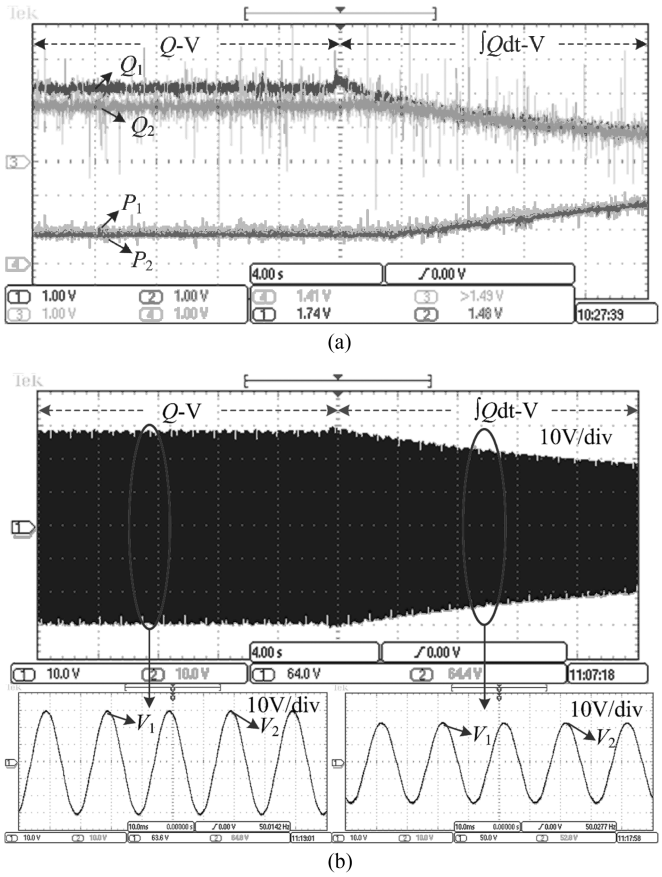

Fig. 18. Comparison of the conventional and improved droop control. (a) Reactive and active powers. (b) Output voltage of the two inverters.

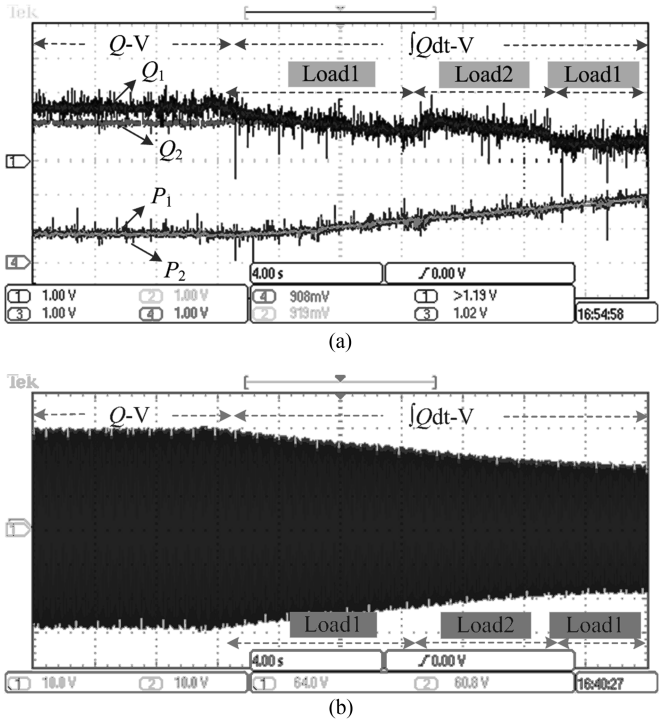

Fig. 19. Reactive power sharing with load step change. (a) Reactive and active powers. (b) Output voltages of the two inverters.

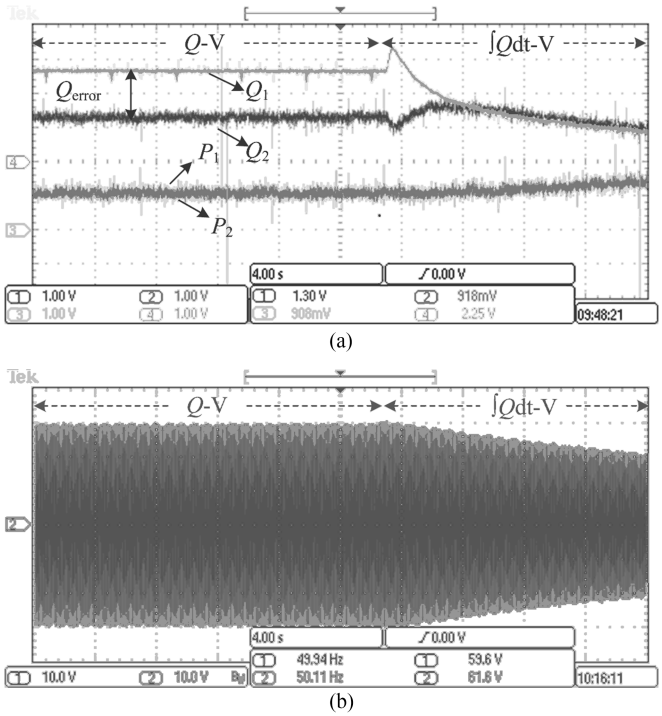

Fig. 20. $\int Qdt - V$ droop method with local load. (a) Reactive and active powers. (b) Output voltages of the two inverters.

error in Fig. 20(a) is much larger under the conventional droop control due to the presence of the local load. Fig. 20(a) implies that the $\int Qdt - V$ droop control can eliminate the reactive power errors with the local load, since the $\int Qdt - V$ droop method functions once there are reactive power errors regardless of the disturbing sources. Fig. 20(b) further illustrates that the reactive power sharing is achieved with the voltage deviation.

B. Voltage Restoration

Since the reactive power sharing is achieved at the price of voltage deviation shown above and the DESUs are responsible to support the voltage in islanded mode, it is necessary to restore the voltage to the acceptable range. Fig. 21 shows the active and reactive powers and the output voltages under the conventional droop control in (5) and (6), $\int Qdt - V$ control in (13), and voltage restoration together with $\int Qdt - V$ control in (15), respectively. The stages of the control methods are also labeled on the top of Fig. 21. From Fig. 21(b), we can see that the voltages are restored to the acceptable range. Meanwhile, the reactive powers in Fig. 21(a) are equally shared.

C. SoC Balancing

In the parallel-connected DESUs, the SoC balancing is one of the critical aspects. Fig. 22 shows the corresponding SoC and the active powers of the two DESUs with different initial SoC under *P-f* and SoC-based *P-f* droop control. The initial SoCs of the two DESUs in (4) are 0.8 and 0.7, respectively. The control stages are labeled on the top of Fig. 22. Under the *P-f* droop control, the active powers are equally shared due to the unified

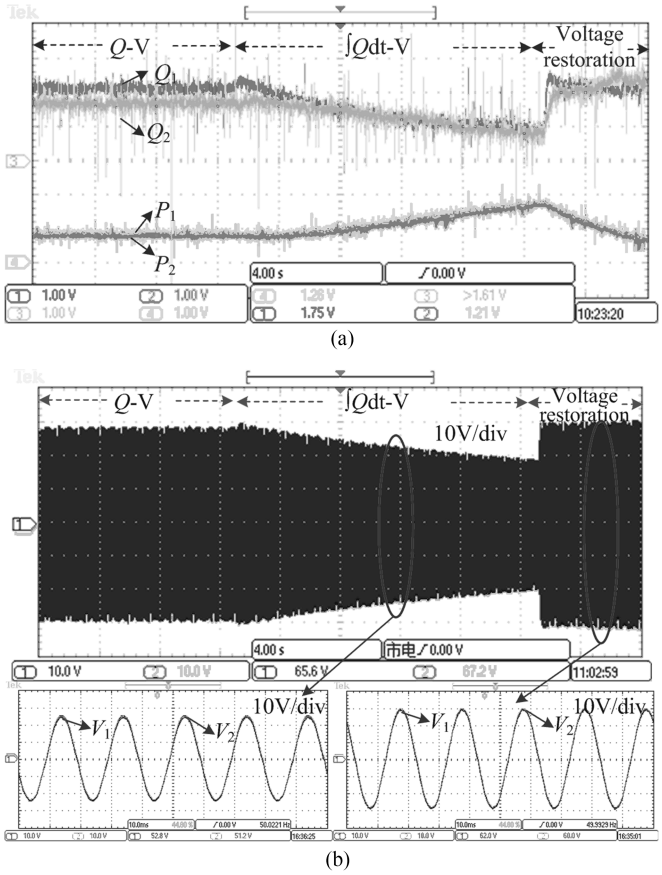

Fig. 21. Reactive power sharing together with voltage restoration. (a) Reactive and active powers. (b) Output voltages of the two inverters.

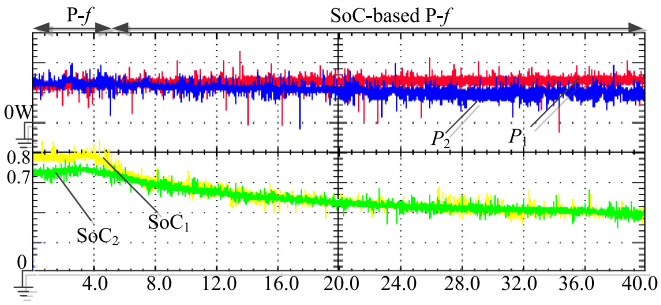

Fig. 22. SoC balancing of the two DESUs.

frequency. However, the SoCs of the two DESUs with different initial SoC are not balanced. Once the SoC-based *P-f* droop control is employed, the active powers of the two DESUs are regulated to achieve SoC balancing. It can be seen from Fig. 22 that the output active power of DESU_1 (P_1) reduces combined with the increase of active power of DESU_2 (P_2), which results from (10) and is helpful to achieve SoC balancing. According to (10), the frequency of the DESU with smaller SoC reduces more and subsequently its output active power decreases more than the others based on (7) and (9). The SoCs of the two DESUs are balanced under the SoC-based *P-f* droop control. Further efforts in terms of several complex conditions about SoC balancing will be made in the next step of our research.

VIII. Conclusion

In this paper, a multifunctional and wireless droop method is proposed to address the problems (SoC unbalancing, reactive power sharing errors, and voltage deviation) confronted by DESUs in autonomous microgrids. The SoC balancing is realized by employing the SoC-based *P-f* droop control which introduces the local measurable SoC of a certain DESU to the conventional *P-f* droop method. The $\int Qdt$–*V* droop method in this paper achieves reactive power sharing through reducing the voltage proportionally to the integration of local reactive power. Besides, a compensation term proportional to the integration of accurately shared active power is introduced to restore the voltage to the acceptable range. Furthermore, a small-signal stability analysis is presented to illustrate the sensitivity of the coefficients in the proposed droop method to the small-signal stability, which determines the values of coefficients to achieve better stability and dynamic performance. The simulation and experimental results demonstrate that the proposed method achieves good results with regard to SoC balancing, power equalization, and voltage restoration. Moreover, the proposed method makes it more viable to form a truly distributed and redundant microgrid, since communications between control layers and multiple DESUs are not necessary in the proposed control strategy.

References

[1] Y. W. Li, D. M. Vilathgamuwa, and P. C. Loh, "Design, analysis, and real-time testing of a controller for multibus microgrid system," *IEEE Trans. Power Electron.*, vol. 19, no. 5, pp. 1195–1204, Sep. 2004.

[2] J. M. Guerrero, L. G. de Vicuña, J. Matas, M. Castilla, and J. Miret, "A wireless controller to enhance dynamic performance of parallel inverters in distributed generation systems," *IEEE Trans. Power Electron.*, vol. 19, no. 5, pp. 1205–1213, Sep. 2004.

[3] C. Wang, C. Sun, Ke. Peng, Y. Li, and Z. Wu, "Study on AC-DC hybrid power flow algorithm for microgrid," *Proc. CSEE*, vol. 33, no. 4, pp. 8–15, Feb. 2013.

[4] Q. Shafiee, J. M. Guerrero, and J. C. Vasquze, "Distributed secondary control for islanded microgrids—A novel approach," *IEEE Trans. Power Syst.*, vol. 29, no. 2, pp. 1018–1030, Feb. 2014.

[5] X. Lu, K. Sun, J. M. Guerrero, J. C. Vasquze, R. Teodorescu, and L. Huang, "Hierarchical control of parallel AC-DC converter interfaces for hybrid microgrids," *IEEE Trans. Smart Grid.*, vol. 5, no. 2, pp. 683–692, Mar. 2014.

[6] X. Lu, K. Sun, J. M. Guerrero, J. C. Vasquze, and L. Huang, "State-of-charge balance using adaptive droop control for distributed energy storage systems in DC microgrid application," *IEEE Trans. Ind. Electron.*, vol. 61, no. 6, pp. 2804–2815, Jun. 2014.

[7] Y. W. Li and C. -N. Kao, "An accurate power control strategy for power-electronics-interfaced distributed generation units operating in a low-voltage multibus microgrid," *IEEE Trans. Power Electron.*, vol. 24, no. 12, pp. 2977–2988, Dec. 2009.

[8] X. Sun and Q. Lǔ, "Improved PV control of grid connected inverter in Low-voltage micro-grid," *Trans. China Electrotech. Soc.*, vol. 27, no. 8, pp. 77–84, Aug. 2012.

[9] J. Li, X. Liang, and X. Chen, "Islanding detection method based on voltage divider for microgrid," *Proc. CSEE*, vol. 30, no. 34, pp. 15–21, Dec. 2010.

[10] A. Mohd, E. Ortjohann, N. Hamsic, and D. Morton, "Challenges in integrating distributed energy storage systems into future smart grid," in *Proc. IEEE Int. Symp. Ind. Electron.*, 2008, pp. 1627–1632.

[11] X. Tan, Q. Li, and H. Wang, "Advances and trends of energy storage technology in microgrid," *Electr. Power Energy Syst.*, vol. 44, pp. 179–191, 2013.

[12] H. Zhou, T. Bhattacharya, and D. Tran, "Composite energy storage system involving battery and ultracapacitor with dynamic energy management in microgrid applications," *IEEE Trans. Power Electron.*, vol. 26, no. 3, pp. 923–191, Mar. 2011.

[13] F. Turki and A. Guetif, "Supporting the low-voltage distribution network with static and mobile energy storage systems," in *Proc. IEEE Int. Multi-Conf. Syst. Signals Devices*, 2013, pp. 1–7.

[14] P.-T. Cheng and T.-L. Lee, "Analysis of harmonic damping effect of the distributed active filter system," *IEEJ Trans. Ind. Appl.*, vol. 126, no. 5, pp. 605–614, Jan. 2006.

[15] X. Tang and Z. Qi, "Energy storage control in renewable energy based microgrid," in *Proc. IEEE Power Energy Soc. Gen. Meet.*, 2012, pp. 1–6.

[16] A. Jamehbozorg, Y. Ye, and R. Sharma, "A robust control approach to smooth output power of wind units using hybrid storage energy systems considering state-of-charge," in *Proc. IEEE PES T&D Conf. Expo.*, 2014, pp. 1–5.

[17] J.-Y. Kim, S.-K. Kim, and J.-H. Jeon, "Coordinated state-of-charge control strategy for microgrid during islanded operation," in *Proc. IEEE Int. Symp. Power Electron. Distrib. Gener. Syst.*, 2012, pp. 133–139.

[18] L. Liu, Y. Wang, and Y. Zhao, "The energy storage system control research based on black-start," in *Proc. IEEE China Int. Conf. Electr. Distrib.*, 2014, pp. 1472–1476.

[19] X. Lu, K. Sun, and J. M. Guerrero, "Double-quadrant state-of-charge-based droop control method for distributed energy storage system in autonomous DC microgrids," *IEEE Trans. Smart Grid.*, vol. 6, no. 1, pp. 147–157, Jan. 2015.

[20] W. Huang and J. A. Abu Qahouq, "Energy sharing control scheme for state-of-charge balancing of distributed battery energy storage system," *IEEE Trans. Ind. Electron.*, vol. 62, no. 5, pp. 2764–2776, May 2015.

[21] W. Huang and J. A. Abu Qahouq, "Distributed energy storage system architecture with energy sharing control for charge balancing," in *Proc. IEEE Appl. Power Electron. Conf.*, 2014, pp. 1126–1130.

[22] X. Zuo and G. Z. Li, "Isolated voltage balancing in super-capacitor energy storage system," in *Proc. Chin. Control Decision Conf.*, 2014, pp. 5124–5128.

[23] F. Altaf, L. Johannesson, and B. Egardt, "Simultaneous thermal and state-of-charge balancing of batteries," in *Proc. IEEE Veh. Power Propulsion Conf.*, Oct. 27–30, 2014, pp. 1–7.

[24] C. Li, T. Dragicevic, J. C. Vasquze, and J. M. Guerrero, "Multi-agent-based distributed state of charge balancing control for distributed energy storage units in AC microgrids," in *Proc. IEEE Appl. Power Electron. Conf.*, 2015, pp. 2967–2973.

[25] C. Li, T. Dragicevic, N. L. Diza, J. C. Vasquez, and J. M. Guerrero, "Voltage scheduling droop control for state-of-charge balance of distributed energy storage in DC microgrids," in *Proc. IEEE Energy Conf.*, 2014, pp. 1310–1314.

[26] D. Wu, F. Tang, T. Dragicevic, J. C. Vasquez, and J. M. Guerrero, "A control architecture to coordinate renewable energy sources and energy storage systems in islanded microgrids," *IEEE Trans. Smart Grid.*, vol. 6, no. 3, pp. 1156–1166, May 2015.

[27] J.-Y. Kim, J.-H. Jeon, S.-K. Kim, C. Cho, J. H. Park, H.-M. Kim, and K.-Y. Nam, "Cooperative control strategy of energy storage system and microsources for stabilizing the microgrid during islanded operation," *IEEE Trans. Power Electron.*, vol. 25, no. 12, pp. 1–12, Dec. 2010.

[28] Y. Xu, W. Zhang, G. Hug, S. Kar, and Z. Li, "Cooperative control of distributed energy storage systems in a microgrid," *IEEE Trans. Smart Grid.*, vol. 6, no. 1, pp. 238–248, Jan. 2015.

[29] D. Shanxu, M. Yu, X. Jian, K. Yong, and C. Jian, "Parallel operation control technique of voltage source inverters in UPS," in *Proc. IEEE Int. Conf. Power Electron. Drive Syst.*, 1999, pp. 883–887.

[30] J. He, Y. W. Li, and J. M. Guerrero, "An islanding microgrid power sharing approach using enhanced virtual impedance control scheme," *IEEE Trans. Power Electron.*, vol. 28, no. 11, pp. 5272–5282, Nov. 2013.

[31] A. Tuladhar, H. Jin, T. Unger, and K. Mauch, "Control of parallel inverters in distributed AC power systems with consideration of line impedance effect," *IEEE Trans. Ind. Appl.*, vol. 36, no. 1, pp. 131–138, Jan./Feb. 2000.

[32] Q. C. Zhong, "Robust droop controller for accurate proportional load sharing among inverters operated in parallel," *IEEE Trans. Ind. Electron.*, vol. 60, no. 4, pp. 1281–1290, Apr. 2013.

[33] J. He and Y. W. Li, "An enhanced microgrid load demand sharing strategy," *IEEE Trans. Power Electron.*, vol. 27, no. 9, pp. 3984–3995, Sep. 2012.

[34] Y. Zhang and H. Ma, "Theoretical and experiment investigation of networked control of parallel operation of inverters," *IEEE Trans. Ind. Electron.*, vol. 59, no. 4, pp. 1961–1970, Apr. 2012.

[35] X. Lu, J. M. Guerrero, K. Sun, and J. C. Vasquez, "An improved droop control method for DC microgrids based on low bandwidth communication

with DC bus voltage restoration and enhanced current sharing accuracy," *IEEE Trans. Power Electron.*, vol. 29, no. 4, pp. 1800–1812, Apr. 2014.
[36] J. M. Guerrero, J. C. Vasquez, J. Matas, L. G. de Vicuña, and M. Castilla, "Hierarchical control of droop-controlled AC and DC microgrids—A general approach toward standardization," *IEEE Trans. Ind. Electron.*, vol. 58, no. 1, pp. 158–172, Jan. 2011.
[37] L. Maharjan, S. Inoue, H. Akagi, and J. Asakura, "State-of-Charge (SOC)-balancing control of a battery energy storage system based on a cascade PWM converter," *IEEE Trans. Power Electron.*, vol. 24, no. 6, pp. 1628–1636, Jun. 2009.
[38] C. K. Sao and P. W. lehn, "Autonomous load sharing of voltage source converters," *IEEE Trans. Power Del.*, vol. 20, no. 2, pp. 1009–1016, Apr. 2005.
[39] H. Kakigano, Y. Miura, and T. Ise, "Distribution voltage control for DC microgrids using fuzzy control and gain-scheduling technique," *IEEE Trans. Power Electron.*, vol. 28, no. 5, pp. 2246–2258, May 2013.
[40] T. Morstyn, B. Hredzak, V. G. Agelidis, and G. Demetriades, "Cooperative control of DC microgrid storage for energy balancing and equal power sharing," in *Proc. Aust. Univ. Power Eng. Conf.*, 2014, pp. 1–6.
[41] R. Majumder, B. Chaudhuri, A. Ghosh, R. Majumder, G. Ledwich, and F. Zare, "Improvement of stability and load sharing in an autonomous microgrid using supplementary droop control loop," *IEEE Trans. Power Syst.*, vol. 25, no. 2, pp. 796–808, May 2010.
[42] S. J. Ahn, J. W. Park, I. Y. Chung, S. I. Moon, S. H. Kang, and S. R. Chung, "Power-sharing method of multiple distributed generators considering control modes and configurations of a microgrid," *IEEE Trans. Power Del.*, vol. 25, no. 3, pp. 2007–2016, Jul. 2010.

Xiaofeng Sun (M'11) received the B.S. degree in electrical engineering from Northeast Heavy Machinery Institute, Heilongjiang, China, in 1993, and the M.S. and Ph.D. degrees in power electronics from Yanshan University, Hebei, China, in 1999 and 2005, respectively.

Since 2008, he has been a Professor at Yanshan University. Also, he is the Director at the Key Laboratory of Power Electronics for Energy Conservation and Motor Drive, Hebei, China. From 2003 to 2007, he was an Associated Professor with Yanshan University. He has authored or coauthored more than 70 transactions and conference papers. His current research interests include dc/dc converters, multiple-input converters, hybrid electric vehicles, microgrids, and power quality control.

Yancong Hao was born in Hebei province, China, in 1990. She received the B.S. degree in electrical engineering from Yanshan University, Qinhuangdao, China, in 2013, where she is currently working toward the M.S. degree in electrical engineering.

Her main research interests include droop control and SoC balancing of distributed energy storage units in microgrids.

Qingfeng Wu was born in Hebei province, China, in 1987. He received the B.S degree in electrical engineering from the Taiyuan University of Science and Technology, Taiyuan, China, in 2011, and the M.S. degree in electrical engineering from the Lanzhou University of Technology, Lanzhou, China, in 2014. He is currently working toward the Ph.D. degree in power electronics and power transmission at Yanshan University, Qinhuangdao, China.

His main research interests include the control of switching power converters, distributed generation, renewable energy interface, microgrids, and power quality.

Xiaoqiang Guo (M'10–SM'14) received the B.S. and Ph.D. degrees in electrical engineering from Yanshan University, Qinhuangdao, China, in 2003 and 2009, respectively.

He has been a Postdoctoral Fellow at the Laboratory for Electrical Drive Applications and Research, Ryerson University, Toronto, ON, Canada. He is currently an Associate Professor at the Department of Electrical Engineering, Yanshan University. He has authored/coauthored more than 50 technical papers, in addition to nine patents. His current research interests include high-power converters and ac drives, electric vehicle charging station, and renewable energy power conversion systems.

Dr. Guo is a Senior Member of the IEEE Power Electronics Society and the IEEE Industrial Electronics Society. He is an active Referee for the IEEE TRANSACTIONS ON SUSTAINABLE ENERGY, the IEEE TRANSACTIONS ON SMART GRID, the IEEE TRANSACTIONS ON INDUSTRIAL ELECTRONICS, and the IEEE TRANSACTIONS ON POWER ELECTRONICS.

Baocheng Wang received the B.S. and M.S. degrees in electrical engineering from Northeast Heavy Machinery Institute, Heilongjiang, China, in 1988 and 1991, respectively, and the Ph.D. degree from Yanshan University, Qinhuangdao, China, in 2008.

Since 2005, he has been a Professor at the Department of Electrical Engineering, Yanshan University. His current research interests include multilevel inverting technology, distributed generation, renewable energy, and fault diagnosis.